

Role of nonlinear toroidal coupling in electron temperature gradient turbulence^{a)}

Z. Lin^{b)} and L. Chen

Department of Physics and Astronomy, University of California, Irvine, California 92697

F. Zonca

Associazione EURATOM-ENEA sulla Fusione, Cassella Postale 65-00044 Frascati, Italy

(Received 19 October 2004; accepted 22 February 2005; published online 9 May 2005)

Global gyrokinetic particle simulation and nonlinear gyrokinetic theory find that electron temperature gradient (ETG) instability saturates via nonlinear toroidal coupling, which is a nonlocal interaction in the wave vector space that transfers energy successively from unstable modes to damped modes preferentially with lower toroidal mode numbers. The electrostatic ETG turbulence is dominated by nonlinearly generated radial streamers. The length of the streamers scales with the device size, which is longer than the distance between mode rational surfaces and electron radial excursions. Both fluctuation intensity and transport level at saturation are independent of the streamer length, and are much smaller than the mixing length estimates.

© 2005 American Institute of Physics. [DOI: 10.1063/1.1894766]

I. INTRODUCTION

Electron temperature gradients in magnetically confined plasmas provide expansion free energy for driving drift wave instabilities,¹ which may induce the high level electron heat transport often observed in toroidal experiments. Identifying the candidate instabilities and understanding the nonlinear interactions are the first step toward predicting and controlling the electron transport in fusion plasmas.

Background. Experimental evidence for the origin of electron transport is not conclusive. Instabilities with a characteristic length on the order of the ion gyroradius, driven by the trapped electron mode (TEM) and/or ion temperature gradient (ITG) mode, have been invoked to account for the anomalous electron transport in ASDEX Upgrade^{2,3} and TCV⁴ tokamaks. On the other hand, the electromagnetic electron temperature gradient (ETG) turbulence with a shorter characteristic length of the collisionless electron skin depth has been suggested as responsible for the electron transport in Tore Supra^{5,6} tokamak. Short wavelength measurement in TFTR tokamak⁷ has observed fluctuations with a characteristic length of the skin depth, however, with a propagation in the ion diamagnetic direction. More recently, diagnostics are being installed in major tokamaks to measure electrostatic ETG fluctuations, which have an even shorter characteristic length of the electron gyroradius and propagate in the electron diamagnetic direction. Large electron transport has also been observed in the absence of strong electron temperature gradient, suggesting mechanisms⁸ not related to the electrostatic drift-wave turbulence.

Linear properties of the toroidal ETG instability⁹ are well understood. The gyro-Bohm level of the ETG electron heat conductivity χ_e^{GB} from a heuristic mixing length estimate¹⁰ is smaller than the ITG ion transport χ_i^{GB} by a

factor of the square root of the electron-to-ion mass ratio, i.e., $\chi_e^{\text{GB}} \sim 1/60 \chi_i^{\text{GB}}$ for deuterium plasmas. Since experimental measurements find, typically, $\chi_e \sim \chi_i$ on the order of χ_i^{GB} , the ETG instability has generally been discarded as a potential driver for the anomalous electron transport. Nonetheless, the nonlinear evolution of ETG and ITG could be very different. Whereas a zonal flow $\mathbf{E} \times \mathbf{B}$ drift nonlinearity^{11–13} dominates in the ITG turbulence, ETG turbulence is regulated by a weaker polarization drift nonlinearity.¹⁴

The renewed interest in the electrostatic ETG instability comes from gyrokinetic continuum simulations using flux-tube geometry,¹⁵ which found that radially extended eddies, or streamers, form in the absence of strong zonal flows and that large electron transport is driven by the electrostatic $\mathbf{E} \times \mathbf{B}$ convection. However, the scale length of ETG streamers is comparable to the simulation box size. This violates the fundamental assumption of the flux-tube simulation,¹⁶ which assumes that the radial correlation length of turbulence eddies is much shorter than the simulation box size and uses a periodic boundary condition in the radial direction. Meanwhile, radially nonlocal, global simulations using fluid models in a small tokamak¹⁷ or a simplified equilibrium geometry¹⁸ found that the ETG turbulent transport is smaller than the flux-tube simulation result by more than an order of magnitude, and concluded that ETG turbulence is unlikely to be responsible for the electron anomalous transport.

Key results from flux-tube simulations¹⁵ of the ETG turbulence are the existence of radial streamers and large electron transport when the magnetic shear is positive. In addition, a mixing length argument was invoked to make the connection between the streamer length and transport level, and a balance between the primary ETG instability and a Kelvin–Helmholtz-type secondary instability¹⁹ was proposed as the saturation mechanism. Furthermore, a conjecture was invoked to argue that the ETG turbulence could survive even in the regime where the ITG/TEM turbulence is suppressed

^{a)}Paper N11 3, Bull. Am. Phys. Soc. 49, 247 (2004)

^{b)}Invited speaker

by strong equilibrium sheared flows. In this conjecture, the condition for the turbulence suppression is that the flow shear $\omega_{\mathbf{E} \times \mathbf{B}} \sim \gamma_0$, where γ_0 is the ETG linear growth rate.

Therefore, the causal relationship between the streamer length and transport level, as well as the mechanism for the instability saturation has not been established by direct numerical simulations or by first-principles theories. Furthermore, the substitution of the nonlinear decorrelation rate by the linear growth rate in the condition for the flow shear suppression²⁰ of ETG turbulence is not supported by theoretical or computational evidence. We address all these issues in our present studies utilizing a well-benchmarked, massively parallel, global gyrokinetic toroidal code¹¹ (GTC) to simulate the electrostatic ETG turbulence in a realistic tokamak.

Findings. Our global gyrokinetic particle simulation and nonlinear gyrokinetic theory find that the ETG instability saturates via nonlinear toroidal coupling, which transfers energy successively from unstable modes to damped modes preferentially with lower toroidal mode numbers. The electrostatic ETG turbulence is dominated by nonlinearly generated radial streamers, which have an eddy turn over time much longer than the linear growth time. Both fluctuation intensity and transport level at saturation are independent of the streamer length, which scales with the device size and is longer than the distance between mode rational surfaces or electron radial excursions. These findings from global simulations with realistic parameters are not consistent with flux-tube simulation results.¹⁵

The nonlinear toroidal coupling found in this study is a novel nonlinear interaction underlying the toroidal spectral cascade. In this nonlinear mode coupling, two unstable high- n pump toroidal eigenmodes with toroidal mode numbers $n_0, n_1 \gg 1$ first drive a low- n quasimode with $n_l = n_0 - n_1 \sim n_0^{1/2}$. Next, the scattering of pump modes on the quasimode creates secondary eigenmodes preferentially with a lower mode number $n_2 = n_1 - n_l$. Then, the coupling of n_0 and n_2 drives another quasimode with a mode number of $2n_l = n_0 - n_2$. This nonlinear process proceeds until all n -matching modes are populated, and results in a downshift of the toroidal spectrum from linearly most unstable modes to nonlinearly dominant modes with lower toroidal mode numbers. This nonlocal interaction in the wave vector space is similar to the Compton scattering with quasimodes playing the role of quasiparticles. Three-mode resonant coupling is not operative due to the frequency mismatch. Similar toroidal spectral cascade occurs in the ITG/TEM turbulence.²¹ Although zonal flows play a dominant role in saturating the ITG/TEM instability, the toroidal spectrum cannot be determined²² solely by interactions between ITG/TEM turbulence and zonal flows. Therefore, the toroidal spectrum of any toroidal drift wave turbulence is ultimately determined by drift-wave–drift-wave interactions. Because of this universal role, nonlinear toroidal couplings represent a new paradigm for plasma turbulence.

Our GTC simulations and associated gyrokinetic theory have important implications for plasma turbulence studies. First, particle dynamics must be treated on the same footing as fluid nonlinearity. Radial streamers, which represent $\mathbf{E} \times \mathbf{B}$ velocity fields, are generated by nonlinear toroidal cou-

plings. Linear wave-particle resonance can be destroyed nonlinearly. Consequently, electron radial excursions are diffusive and much shorter than the streamer size, i.e., particles and fluid elements do not move together due to the parallel free streaming motion. While wave-wave couplings determine fluctuation characteristics, transport is driven by wave-particle interactions. This is a crucial difference with fluid turbulence, where fluid elements move with velocity fields. Fluid concepts, such as mixing length rule and eddy turnover time, do not correctly describe transport processes in collisionless plasma turbulence. Second, toroidal geometry must be treated rigorously in studying toroidal drift-wave turbulence. The nonlinear toroidal coupling is strictly a geometry-specific effect because two parallel streamers cannot interact in the slab geometry. All eigenmodes participate in nonlinear toroidal coupling. Thus, the saturation amplitude may not be predicted accurately using a small number of modes. Finally, the contradictory results from ETG turbulence simulations between flux-tube and global codes are presumably consequences of differences in the respective geometry representations. While the toroidicity is treated rigorously in global codes, flux-tube codes make key approximations, the validity regime of which remains dubious for nonlinear simulations involving fluctuations with low toroidal mode numbers and nonlinear particle dynamics.

The paper is organized as follows. Global GTC simulations of electrostatic ETG turbulent transport is presented in Sec. II. In Sec. III, we discuss the saturation of ETG instability via nonlinear toroidal couplings, as observed in GTC simulations. The gyrokinetic theory of nonlinear toroidal couplings is presented in Sec. IV. Discussions and conclusions are in Sec. V.

II. ETG TURBULENT TRANSPORT

Our studies utilize a well-benchmarked, massively parallel, full torus GTC.¹¹ Both linear and nonlinear wave-particle resonances, and finite Larmor radius effects are treated in gyrokinetic particle simulations.²³ Toroidal geometry is treated rigorously using magnetic coordinates which provide the most general coordinate system for any magnetic configuration possessing nested surfaces. The straight field lines are desirable for describing the microinstabilities with field-aligned mode structures and for efficiently integrating the electron and ion orbits. A challenge for full torus ETG turbulence simulations is that the computational cost grows rapidly with the device size. Global ETG turbulence simulations only became feasible with an efficient global field-aligned mesh,²¹ which provides the highest possible computational efficiency without any simplification in terms of physics models or simulation geometry. Consequently, the GTC code has a unique feature that the number of computations N_c has a quadratic, rather than the usual cubic, dependence on the device size, i.e., $N_c \sim (a/\rho_e)^2$, where a is the tokamak minor radius and ρ_e is the electron gyroradius. This reduces computational requirements by three orders of magnitude for realistic ETG turbulence simulations. Furthermore, the particle-in-cell approach efficiently resolves the five-dimensional (5D) phase space through a Monte Carlo

sampling,²⁴ which reduces the number of velocity grids compared to that in continuum codes. As a result, all unstable toroidal modes are treated in the global GTC code. Finally, effective utilization of massively parallel computers allows nonlinear ETG simulation using billions of spatial grids and particles.

All simulations reported in this paper use representative parameters of tokamak plasmas which have a peak electron temperature gradient at $r=0.5a$ with the following local electron parameters: $R_0/L_T=6.9$, $R_0/L_n=2.2$, $q=1.4$, $\hat{s}\equiv(r/q)\times(dq/dr)=0.78$, $T_e/T_i=1$, and $a/R_0=0.36$. Here R_0 is the major radius, L_T and L_n are the electron temperature and density gradient scale lengths, respectively, T_i and T_e are the ion and electron temperatures, and q is the safety factor. Our global simulations use fixed boundary conditions with electrostatic potential $\delta\phi=0$ enforced for $r<0.25a$ and $r>0.75a$. Modes with short perpendicular wavelength ($k_\perp\rho_e>1$) are filtered out, where $\rho_e=v_e/\Omega_e$, $v_e=\sqrt{T_e/m_e}$ with Ω_e the electron cyclotron frequency and m_e the electron mass. Simplified physics models include a parabolic profile $q=0.854+2.184(r/a)^2$, a temperature gradient profile of $\exp\{-[(r-0.5a)/0.2a]^6\}$, a circular cross section, and electrostatic fluctuations with an adiabatic ion response. Extensive studies of numerical convergence have been carried out using relatively small device size with perpendicular grid sizes of $(1-2)\rho_e$, (45-90) parallel grids per toroidal connection length, (5-20) particles per cell, and time steps $(0.1-0.2)L_T/v_e$. The verification of true convergence is especially challenging for the simulations of ETG turbulence due to the large ratio of the device size to the fluctuation scale length. Nevertheless, the key nonlinear physics found in this study, i.e., ETG saturation and transport mechanisms, has been carefully benchmarked to be free of numerical convergence issues.

The linear ETG dispersion relation for these plasma parameters shows that the most unstable mode has a poloidal wave vector $k_\theta\rho_e=0.33$ with a linear growth rate $\gamma_0=0.038v_e/L_T$ and a real frequency $\omega_r\approx 3\gamma_0$. The growth rate decreases to $\approx\gamma_0/4$ at $k_\theta\rho_e=0.1$ and 0.6. The real frequency is roughly a linear function of k_θ for $k_\theta\rho_e\leq 0.6$.

In fully nonlinear simulations, random fluctuations with a very small amplitude first grow exponentially, then saturate, and eventually reach a quasisteady state. In the toroidal spectra shown in Fig. 1, each mode is represented by the amplitude of the harmonics (n,m) with a toroidal mode number n and a poloidal mode number m such that $k_\theta=nq/r$, $m=nq$, and $q=1.4$ at $r=0.5a$. In the linear phase, the spectrum peaks at $k_\theta\rho_e\approx 0.3$ and decreases to very low amplitude at $k_\theta\rho_e\approx 0.2$ and 0.4. The spectral width is narrower than that of the linear growth rate as expected in an initial value calculation. In the nonlinear phase, the toroidal spectrum gradually downshifts to peak near $k_\theta\rho_e\approx 0.1$ with long wavelength modes down to $k_\theta\rho_e=0$ all excited. Similar nonlinear downshift of the toroidal spectrum also occurs in the ITG turbulence.²¹ Therefore, we conjecture that toroidal spectral cascades in both ETG and ITG turbulence are governed by same processes, i.e., nonlinear toroidal couplings.

In the time history of three representative modes shown in Fig. 2, the linearly most unstable short wavelength mode

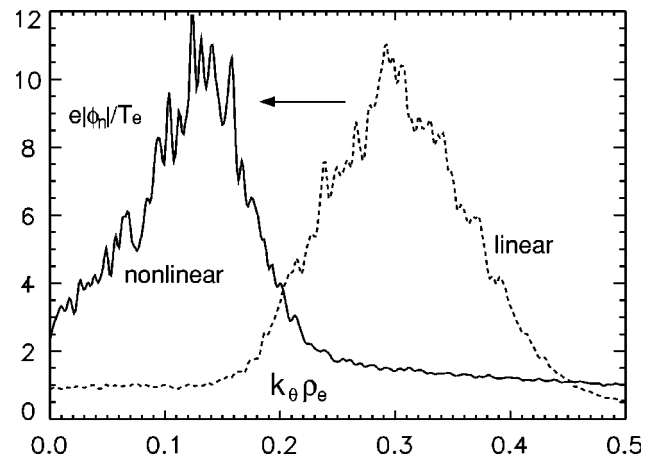


FIG. 1. ETG fluctuation spectra in linear phase ($\times 10^5$, dotted) and at $t \approx 20/\gamma_0$ after saturation ($\times 10^4$, solid) for $a=2000\rho_e$.

grows first to a high amplitude, then saturates, and decreases to a low level. The longer wavelength modes have two growth phases: first a fast growth and then a much slower growth after the most unstable short wavelength mode amplitude decreases. The fast growth in the first phase is nonlinearly driven since the growth rates are much larger than the linear growth rates of the long wavelength modes. This suggests that the short wavelength mode saturates via a nonlinear mode coupling to the longer wavelength modes. The saturated amplitude of the long wavelength modes are much higher than that of the linearly most unstable modes, showing that the structures in the fully developed ETG turbulence are nonlinearly generated. Finally, an important clue for the ETG nonlinear physics is that the very long wavelength mode with $k_\theta\rho_e=0.02$ grows before the shorter wavelength mode with $k_\theta\rho_e=0.15$, suggesting that the downshift of the toroidal spectrum is not the conventional inverse cascade,¹⁴ in which the fluctuation energy flows orderly from short to long wavelengths due to local interactions in n -space.

The structure of the fully developed ETG turbulence is shown in Fig. 3, which is a poloidal contour plot of the electrostatic potential (or density). The seemingly coherent structure in Fig. 3 actually contains hundreds of toroidal

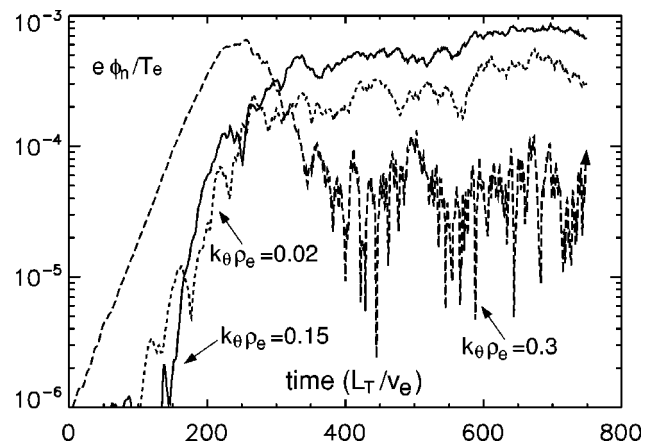


FIG. 2. Time history of three toroidal modes with $k_\theta\rho_e=0.3$ (dashed), 0.15 (solid), and 0.02 (dotted).

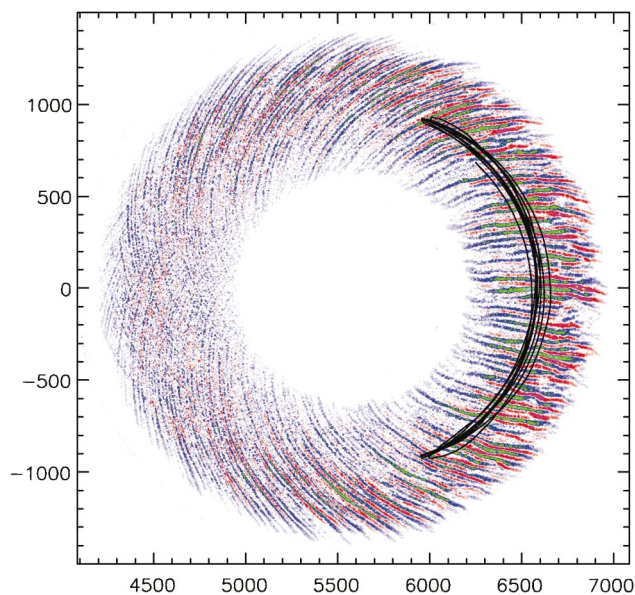


FIG. 3. (Color). Poloidal contour plots of electrostatic potential at $t \approx 20/\gamma_0$ after saturation. The poloidal projection of a typical electron orbit from saturation to t is plotted. The length unit is ρ_e .

modes as shown in the nonlinear spectrum of Fig. 1. Clearly, the ETG turbulence is dominated by nonlinearly generated radial streamers. By varying the simulation device size, we find that the radial streamer length scales with the device size. This is in sharp contrast to the isotropic eddies of the ITG turbulence,²¹ where the shearing effects of spontaneously generated zonal flows break up the linear toroidal ITG eigenmodes.

The nonlinear decorrelation rate γ_{nl} is conventionally estimated from streamer eddy turnover time associated with $\mathbf{E} \times \mathbf{B}$ drift, $\gamma_{nl} \sim \Omega_e k_r \rho_e k_\theta \rho_e e \delta \phi / T_e$. Using streamer envelope $k_r \rho_e \sim 4 \times 10^{-3}$, $k_\theta \rho_e \sim 0.1$, and $e \delta \phi / T_e \sim 8 \times 10^{-3}$, we find that $\gamma_0 / \gamma_{nl} \sim 16$ for the case of $a = 2000 \rho_e$. Note that the value of γ_0 / γ_{nl} increases linearly with a / ρ_e since both $k_r \rho_e$ and $e \delta \phi / T_e$ are proportional to ρ_e / a . Therefore, the nonlinear decorrelation rate γ_{nl} is much smaller than the linear growth rate γ_0 , contradicting the mixing length rule that the instability saturates when γ_{nl} balances γ_0 . The fact that $\gamma_0 / \gamma_{nl} \gg 1$ also invalidates a common practice, where γ_{nl} is replaced by γ_0 in the condition for the turbulence suppression by sheared $\mathbf{E} \times \mathbf{B}$ flows, i.e., $\omega_{\mathbf{E} \times \mathbf{B}} \sim \gamma_0$. An assumption of $\gamma_{nl} \sim \gamma_0$ is a key element of the conjecture¹⁵ that the ETG turbulence could survive when strong sheared flows suppress the ITG/TEM turbulence in some tokamak operation regimes.

A mixing length type of argument has been invoked to attribute the large electron transport observed in flux-tube simulations¹⁵ to the convection of plasma by the radial streamers. However, electrons do not rotate around the streamers, as illustrated by a typical electron orbit during a period of $20/\gamma_0$ in Fig. 3. This is due to the fact that electrons move predominantly along the magnetic field line and resonant electrons, which contribute to the transport, can decorrelate with streamers due to the overlapping of phase-space islands or the nonlinear loss of the parallel resonant

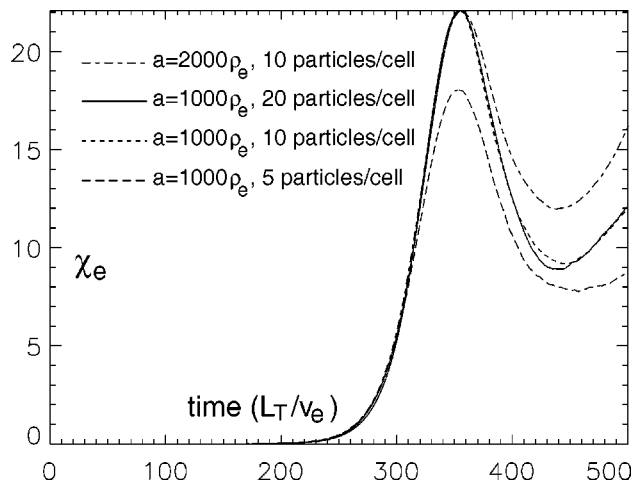


FIG. 4. Time history of the heat conductivity.

condition. Thus, we find that streamers only cause a small perturbation on the electron free streaming motion. To further demonstrate that the electron thermal transport is diffusive, it is instructive to examine the statistics of radial excursions of test particles.²¹ The test particles have a Maxwellian distribution with a temperature of T_e and move under the influences of the fluctuating potential. After an initial ballistic motion over a short radial distance, the volume averaged electron radial excursion is diffusive. The range of the radial excursion is only about one-tenth of the streamer size. During the same period, ETG streamers should have completed a full rotation as estimated by the eddy turnover time. Again, this result supports the thesis that transport is induced by the overlapping of phase-space islands of resonant electrons, and further invalidates the transport scaling obtained from the mixing length estimate, which assumes that particles rotate around turbulence eddies. Plasma turbulence eddies are simply amplitude contours of electrostatic potential (or density) perturbations, or equivalently, $\mathbf{E} \times \mathbf{B}$ velocity fields. Due to free streaming motion along the magnetic field line in collisionless plasmas, particles do not only move with the velocity fields. In contrast, the fluid elements move exactly with the velocity fields in the fluid turbulence because the collisional mean free path is typically much shorter than the fluctuation scale length.

The electron heat conductivity χ_e (in gyroBohm unit $v_e \rho_e^2 / L_T$) at saturation is indeed insensitive to the device size (and thus the streamer length). In Fig. 4, volume averaged χ_e is very similar for $a / \rho_e = 1000$ and 2000. The fluctuation intensity in gyroBohm unit is also found to be insensitive to the device size. Therefore, in contrast to the conventional wisdom, we find no direct causal relationship between the streamer length and the electron transport level, and that the transport is well below that expected from the mixing length estimates. This is obviously due to the fact that transport is diffusive and driven by the local fluctuation intensity.²⁵ Meanwhile, the intensity is determined by the saturation mechanism, i.e., nonlinear toroidal coupling which is not sensitive to the streamer length. We emphasize here the size scaling of χ_e at saturation. Even the large χ_e at the early

nonlinear stage is an order of magnitude smaller than the ITG/TEM transport with the same plasma parameters.²⁸ After the initial saturation, the electron heat conductivity evolves slowly and reaches a much lower level,^{26,27} a process that is not well understood.

For comparisons with flux-tube simulations, we made several simplifications, i.e., neglecting the Debye shielding term in the gyrokinetic Poisson equation,²³ using marker particles with uniform temperature in the partially linearized δf scheme²⁹ which removes parallel nonlinearity,³⁰ assuming no externally driven flows, and neglecting the coupling to ITG/TEM turbulence.³¹ All these additional effects could further reduce the ETG electron transport. Numerical convergence studies indicate that 10 particles per cell are sufficient for a few tens of linear growth times after nonlinear saturation. Nevertheless, nonlinear interactions involving fine scale structures in phase-space are difficult to resolve in particle simulations, on the other hand, are artificially destroyed in continuum simulations using coarse velocity grids. Therefore, all these physics subtleties and the issue of numerical noise buildup in long time δf simulation^{26,27,32} need to be further examined in order to quantitatively predict the ETG electron transport level.

III. NONLINEAR TOROIDAL COUPLING

In order to understand why fluctuation intensity and electron transport are independent of the streamer length, we need to study the saturation mechanism for the toroidal ETG instability. The linear eigenmodes can be described with three degrees of freedom: a toroidal eigenmode number n assuming axisymmetry, a parallel mode structure determined by the radial width of the poloidal mode number m , and a ballooning angle θ_0 representing the radial envelope of the linearly coupled m harmonics. Correspondingly, nonlinear interactions can take the following three forms: a nonlinear mode coupling between two n toroidal eigenmodes, a modification of the parallel mode structure, and a modulation of the radial envelope. The envelope modulation, i.e., the generation of zonal flows, dominates in the ITG turbulence. In the ETG turbulence, all these interactions are formally on the same order.

The simulation results reported in Sec. II suggest that nonlinear mode coupling plays a key role in regulating the ETG turbulence. We study all these interactions and find that the coupling of two n eigenmodes, labeled as nonlinear toroidal coupling, is the dominant nonlinear interaction in the ETG turbulence. All simulations in this section use the same parameters described in Sec. II except that the tokamak size is $a=1000\rho_e$ with a simulation domain of $r/a=[0.4, 0.6]$. All diagnostics in this section are at a reference minor radius $r=0.5a$ with a safety factor $q=1.4$.

A. Saturation of a single toroidal eigenmode

It has been suggested that ETG instability saturates when the linear growth of the primary ETG instability is balanced by a slablike secondary Kelvin–Helmholtz (KH) instability.¹⁵ In this process the linear streamer of a single toroidal eigenmode is broken up by the KH instability. To test this hypoth-

esis, we first study the nonlinear saturation of a single toroidal eigenmode of $n_0=110$ with $k_{\theta}\rho_e=0.31$. In this test case, we initially only allow the n_0 mode to grow from very small random noise, i.e., only the electric field associated with this mode is used in the calculation of particle orbits. The poloidal contour plot of density perturbation shows that the mode is dominated by an eigenmode with a ballooning angle $\theta_0=0$. The linear streamers^{19,26,33,34} are formed by linear toroidal couplings, where many poloidal m harmonics of a single n mode are linearly coupled because of the magnetic field dependence on the poloidal angle. At $r=0.5a$, the dominant m harmonic is $m_0=qn_0=154$. When the amplitude of n_0 mode is much higher than any other mode, all n modes are allowed to grow. After saturation of the $n_0=110$ mode, the linear streamer is well preserved. We do not find the signature of the secondary KH instability. This is in contrast to the ITG where zonal flows, generated through a secondary instability, breakup linear ITG streamers.

At the saturation of the pump eigenmode, two most significant secondary modes at $r=0.5a$ are that of $n=0$, $m=\pm 1$, or $(0, 1)$ mode, and $n=2n_0=220$, $m=2m_0\pm 1=307, 309$, or $(2n_0, 2m_0\pm 1)$ mode. They are evidently generated by the following mode coupling process:

$$(n_0, m_0) + (n_0, m_0 \pm 1) \Rightarrow (0, \pm 1), (2n_0, 2m_0 \pm 1).$$

This coupling can be easily identified in the upper panel of Fig. 5, which shows the amplitude of the m harmonics in a linear ETG toroidal eigenmode as a function of the radial coordinate denoted by the safety factor $q(r)$. Each m harmonic peaks at the mode rational surface where $m=qn_0$ and decreases to very low amplitudes at neighboring mode rational surfaces for $m\pm 1$ harmonics. The radial width of m harmonics represents the parallel mode wave vector k_{\parallel} . The wider radial width corresponds to the larger k_{\parallel} . The radial profile of the m harmonics after nonlinear saturation in the middle panel of Fig. 5 clearly shows a widening of the m harmonics, i.e., an increase in k_{\parallel} . Landau damping is then enhanced since the ETG linear frequency is larger than the transit frequency of thermal electrons. Therefore, the single- n ETG eigenmode could saturate through the modification of the parallel mode structure via a coupling to the $(0, 1)$ mode, which is of particular interest since all linearly unstable modes contribute to it in the fully nonlinear simulations. The radial coherence length of the $(0, 1)$ mode is similar to the distance between mode rational surfaces of the high- n pump mode, as shown in the lower panel of Fig. 5, and thus the assumption of an adiabatic ion response is valid even for the $n=0$ mode. Meanwhile, the zonal flow, or $(0, 0)$ mode, is generated through modulation of the radial envelope. However, the amplitude of zonal flow is low and it does not breakup the linear ETG streamer.

B. Saturation in the presence of multiple eigenmodes

We now study the nonlinear interaction between two n modes by adding another pump mode. We find that the saturation amplitude of a single- n mode is much higher than that in the presence of another eigenmode with a similar ampli-

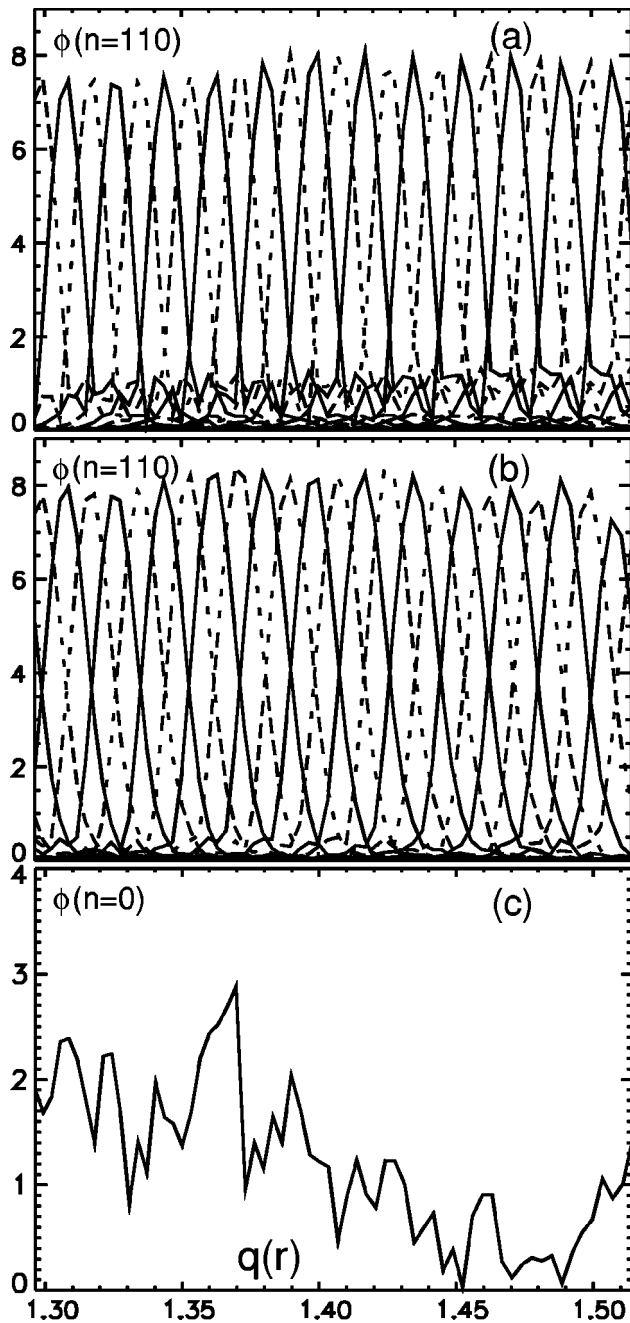


FIG. 5. Radial profiles of (n,m) harmonics of $e|\phi|/T_e$ for $n_0=110$ before (panel a, $\times 10^6$) and after (panel b, $\times 10^3$) saturation, and for $(0,1)$ mode (panel c, $\times 10^4$) before saturation. Each solid or dashed line describes an m harmonic.

tude, suggesting that the nonlinear coupling between two eigenmodes is the dominant process in the ETG saturation.

Since the most unstable toroidal eigenmodes typically have an envelope $k_r=0$, a conceptual difficulty we must first address regarding nonlinear mode couplings is whether two toroidal eigenmodes with $k_r=0$ can nonlinearly interact. Two streamers in a slab geometry with parallel wave vectors would not nonlinearly interact due to the fact that $\mathbf{k}_1 \times \mathbf{k}_2 = 0$. This concept of slab streamers has perhaps misled previous studies of toroidal drift-wave turbulence. In fact, the situation is quite different for toroidal eigenmodes. Although toroidal streamers have an envelope $k_r=0$, there is a “hid-

den” $k_r = \delta \theta k_\theta$ due to the localization of each m harmonics near the mode rational surface as shown in Fig. 5. This can also be visualized in a poloidal contour plot of the superposition of two toroidal eigenmodes, which shows fine radial structures away from the poloidal angle $\theta=0$. Therefore, two toroidal eigenmodes can nonlinearly interact because of the unique ballooning mode structure. This nonlinear streamer coupling is strictly geometry specific since there is no slab counterpart. We thus call the nonlinear coupling between two n modes a nonlinear toroidal coupling.

We now examine the nonlinear toroidal coupling of two n modes. Two toroidal eigenmodes, $n_0=110$ and $n_1=95$, are allowed to grow first, i.e., only these two pump modes feed back to the particle dynamics. When the amplitudes of these two modes are much higher than any other mode, all toroidal modes are allowed to grow. The radial profiles of these two eigenmode in linear phase are shown in the upper two panels of Fig. 6. Each m_0 harmonic of the n_0 mode, in addition to the coupling to the $m_0 \pm 1$ harmonics of the n_0 mode itself, interacts most strongly with one m_1 harmonic of the n_1 mode, where m_0 and m_1 are the harmonics whose mode rational surfaces sit close to each other. The coupling proceeds,

$$(n_0, m_0) + (n_1, m_1) \Rightarrow (n_0 \pm n_1, m_0 \pm m_1).$$

This coupling produces both a very high- n mode, $n_h = 205$, and a low- n mode, $n_l = 15$. The amplitude of the very high- n mode is much smaller since the coupling coefficients of the n_h mode is much weaker than that to the n_l mode. This is because the intrinsic frequency, i.e., the inertia, of the n_h mode is much higher than that of the n_l mode, and because the interacting wave vectors of the two pump eigenmodes are almost parallel in the coupling to the n_h mode, whereas they are almost perpendicular in the coupling to the n_l mode. The low- n mode is a forced oscillation, i.e., a quasimode, since its intrinsic frequency is much smaller than the frequency difference between the two pump eigenmodes, which is on the order of their linear growth rates. As shown in the lower panel of Fig. 6, each m harmonic of the low- n quasimode is localized near its own mode rational surface, and the radial coherence length of the quasimode is similar to the distance between the mode rational surfaces of pump modes, which is the radial width of the interactions between m harmonics. This is also confirmed in a poloidal contour plot, which shows that the radial eddy size of the quasimode is very small. Therefore, the quasimode does not possess the ballooning mode structure and has a very long parallel wavelength, $k_{\parallel} \sim 1/qR_0 n_0^{1/2}$ (Sec. IV), near mode rational surface. Resolving these low- n quasimodes with very long parallel wavelength would require¹⁶ simulation box size orders of magnitude bigger than typical ETG flux-tube simulations.¹⁵

The generation of the low- n quasimode, $n_l = n_0 - n_1 = 15$ is just the first step of the nonlinear toroidal coupling. The quasimode n_l couples back to the two pump modes and generates secondary n_2 modes, $n_1 - n_l = 80$, and $n_0 + n_l = 125$ (upper panel of Fig. 7) before the saturation of pump modes. In turn, each secondary n_2 mode couples with the far-side pump mode to generate another quasimode $n_l = 30$. Then, the coupling between the low- n quasimode $n_l = 30$ with the pump modes generates further secondary modes $n_2 = 65$ and 140.

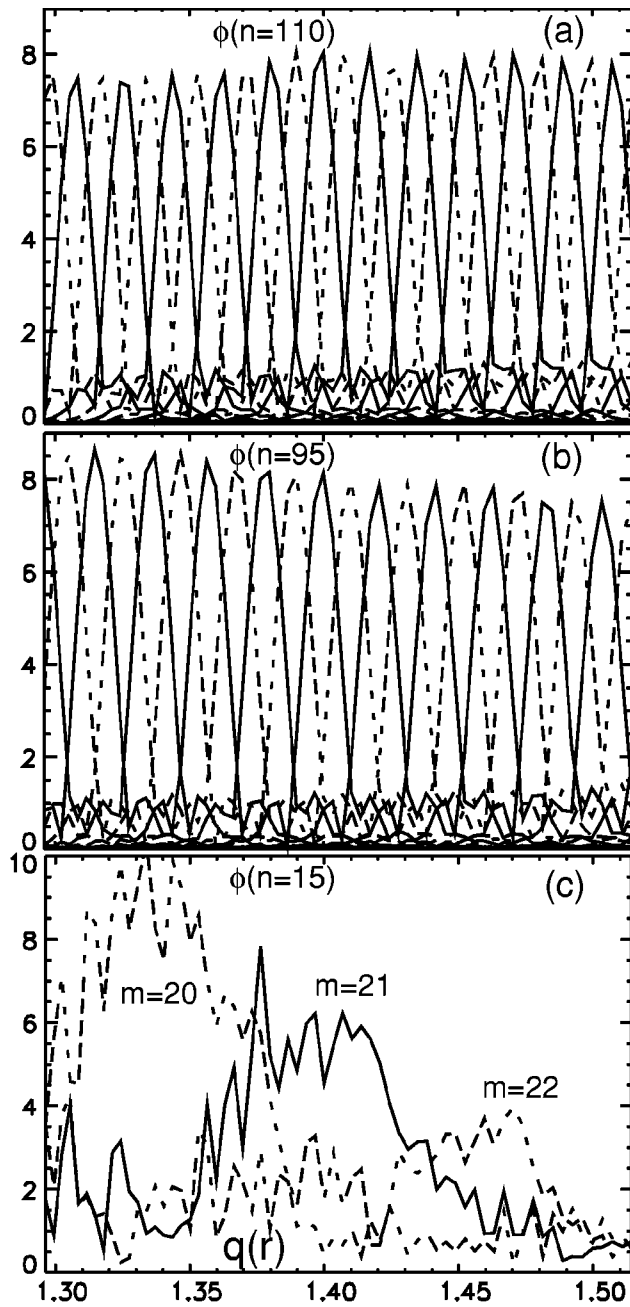


FIG. 6. Radial profiles of (n, m) harmonics of $e|\phi|/T_e$ for $n_0=110$ (panel a, $\times 10^6$), $n_1=95$ (panel b, $\times 10^6$), and $n_l=15$ (panel c, $\times 10^5$) before saturation. Each solid or dashed line describes an m harmonic.

These successive coupling processes proceed until all n modes that satisfy the n -matching condition are populated with either a quasimode or a secondary mode, as shown in the middle panel of Fig. 7 after the saturation of pump modes. The amplitudes of the higher- n secondary modes, $n_2=125, 140, \dots$, are much smaller than lower- n secondary modes, $n_2=80, 65, \dots$. This indicates that the energy cascades preferentially to lower- n secondary modes. Each coupling always involves a quasimode, a secondary ballooning mode and a pump ballooning mode. The low- n quasimodes do not contain much energy or drive much transport. Rather, they act as mediators that facilitate the transfer of energy from pump modes to secondary modes. Thus, the nonlinear

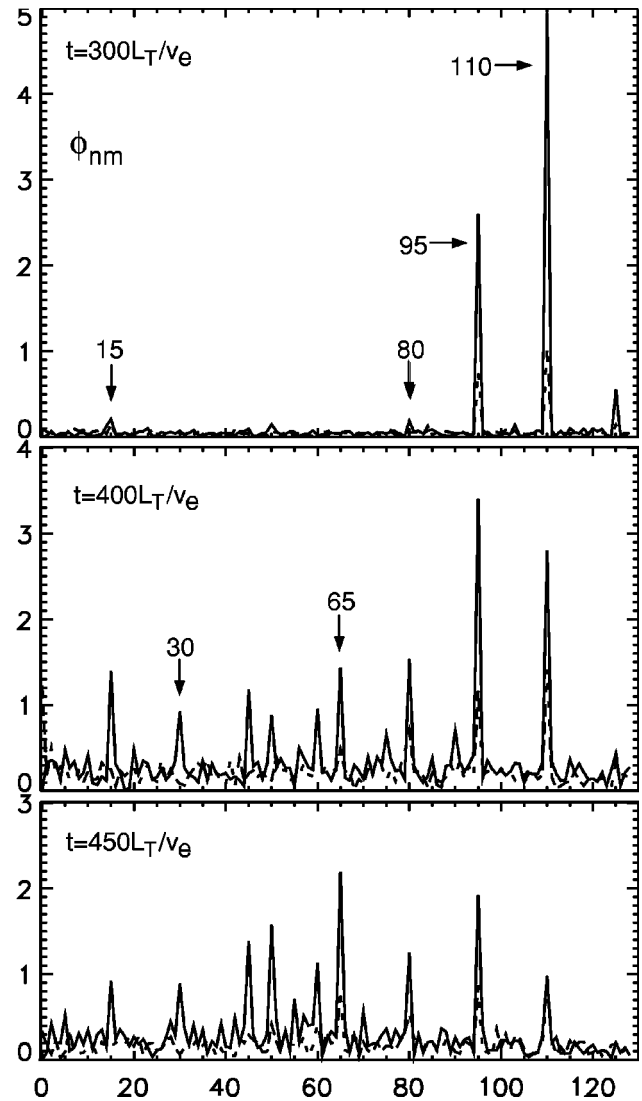


FIG. 7. Toroidal mode number n spectra before and after saturation of the pump modes at $r=0.5a$. Solid line represents the harmonics of $m=qn$; $m=qn+1$ for dashed line.

toroidal coupling can be viewed as a two-step process, first the generation of the low- n quasimode, and the subsequent energy transfer from pump modes to lower- n secondary modes. The second step is similar to the Compton scattering³⁵ with the quasimode playing the role of the quasiparticle.

The parallel mode structure of pump modes is also modified at saturation through coupling to the $(0, 1)$ harmonic (middle panel of Fig. 6). However, its amplitude decreases quickly due to Landau damping (lower panel of Fig. 6). The amplitude of the zonal flow, or $(0, 0)$ mode, is always very small, consistent with the fact that the envelope modulation is insignificant. At the steady state, the ETG turbulence is dominated by nonlinearly-generated lower- n secondary mode streamers, which have longer intrinsic characteristic time scales and could be prone to the shearing effects of the equilibrium and zonal flows. Steady state is achieved both via energy transfer to damped modes and via modification by

the (0, 1) mode of the parallel mode structure of linearly unstable modes, which enhances Landau damping.

In summary, we find that the toroidal ETG instability saturates via nonlinear toroidal couplings, which transfer energy from unstable to stable modes. The parallel wave vector also increases through coupling to the (0, 1) mode, which is a weaker nonlinear interaction due to Landau damping of the (0, 1) mode. Finally, the generation of the zonal flow is the weakest nonlinear interaction because the amplitude of the sidebands with $\theta_0 \neq 0$ is much smaller than those of the pump eigenmodes.

IV. GYROKINETIC THEORY OF NONLINEAR TOROIDAL COUPLING

In this section, we develop a gyrokinetic theory of the nonlinear toroidal coupling. To delineate the mode-coupling process, let us first consider the nonlinear couplings between three modes with toroidal mode number n_0 , n_1 , and n_l . Thus, we have in mind, $n_0 \sim n_1 \sim O(10^3) \gg 1$ being the spontaneously excited ETG modes (pump waves) and $n_l = n_0 - n_1 \sim O(n_0^{1/2}) > 1$ being the low- n beat mode. In addition, noting that ETG normal mode real frequency ω_0 scales linearly with n_0 (Sec. II), we adopt the following frequency and wavelength ordering: $1 > \gamma_0/\omega_0 \sim \gamma_1/\omega_1 \sim k_\perp \rho_e \sim n_0^{-1/4} > |\omega_0 - \omega_1|/|\omega_0| \sim n_0^{-1/2}$, which will be used in the following to solve the electron nonlinear gyrokinetic equation in the fluid limit.

Within the three-wave coupling model, we have,

$$\delta\phi(\vec{r}, t) = \delta\phi_0(\vec{r}, t) + \delta\phi_1(\vec{r}, t) + \delta\phi_l(\vec{r}, t) + \text{c.c.},$$

where $\delta\phi_0$ and $\delta\phi_1$ take the following ballooning-mode representation,³⁶ assuming circular magnetic surfaces and (r, θ, ζ) being a right handed toroidal flux coordinate system:

$$\delta\phi_0(\vec{r}, t) = e^{-in_0\zeta} A_0(t) \sum_{m_0} e^{im_0\theta} \Phi_0(n_0q - m_0),$$

$$\delta\phi_1(\vec{r}, t) = e^{-in_1\zeta} A_1(t) \sum_{m_1} e^{im_1\theta} \Phi_1(n_1q - m_1),$$

$$\delta\phi_l(\vec{r}, t) = e^{-i(n_l\zeta - m_l\theta)} A_l(t) \sum_j e^{ij\theta} \Phi_{lj}(\vec{r}).$$

We have thus ignored envelope modulations due to either equilibrium variations or zonal flow dynamics, which occurs at a longer time scale for ETG.

In fact, the crucial difference between ITG and ETG zonal flow dynamics is that massless electron zonal response is identically zero in the ITG case, whereas large orbit ion zonal dynamics is adiabatic for ETG. For this reason, the ETG zonal flow polarization will be different, i.e., an $O(k_z^{-2} \rho_e^{-2})$ larger, with respect to that of ITG (Ref. 37) and zonal flow dynamics will occur on a $O(k_z^{-2} \rho_e^{-2})$ longer time scale with respect to the toroidal three-wave couplings discussed here. Here, k_z is the wave vector of the zonal flow. Contrary to ITG, where zonal flows interactions with a coherent ITG determine the shortest nonlinear time scale, ETG nonlinear dynamics is dominated by nonlinear scattering processes to longer wavelengths, via a truly toroidal process, as

demonstrated in the global GTC simulations. In the following, we derive analytic expressions for the parallel mode structures of the low- n beat mode and construct nonlinear evolution equations for the local amplitudes, $A_0(t)$, $A_1(t)$, and $A_l(t)$.

Due to the radially localized nature of Φ_0 and Φ_1 , effective nonlinear coupling requires that significant spatial overlap exists between the poloidal mode structures of the two considered ETG pump waves. This fact, in turn, can be expressed as a *selection rule* via Φ_0 and Φ_1 representation. In other words, assuming r_s as the reference low-order mode rational surface, i.e., $q(r_s) = m_l/n_l$, $\delta\phi_{0,1}$ can be further expressed as, in the large $n_{0,1}$ asymptotic limit,

$$\delta\phi_{0,1}(\vec{r}, t) = e^{-i(n_{0,1}\zeta - m_{s,0,1}\theta)} A_{0,1}(t) \sum_j e^{ij\theta} \Phi(z_{0,1} - j),$$

with $m_{s,0,1} = n_{0,1}q(r_s)$, $z_{0,1} = (r - r_s)/\Delta_{0,1}$, and $\Delta_{0,1} = 1/n_{0,1}q'(r_s)$.

The governing field equation is the quasineutrality condition, for $k = 0, 1, l$, assuming that ion response is adiabatic (since $k_\perp \rho_i \sim \sqrt{m_i/m_e} k_\perp \rho_e \gg 1$),

$$\frac{eN_{e0}}{T_e} (1 + \tau) \delta\phi_k + \langle J_{0k} (\delta g_k^{\text{linear}} + \delta g_k^{\text{nl}}) \rangle_{\vec{v}} = 0, \quad (1)$$

where $\tau = T_e/T_i$, and N_{e0} is the electron (ion) equilibrium density, $\langle \rangle_{\vec{v}}$ denotes integration in velocity space, and δg_k 's satisfy the electron nonlinear gyrokinetic equations,³⁸

$$L_g \delta g_k^{\text{linear}} = -\frac{e}{T_e} F_M (\partial_t + i\omega_*) J_0 \delta\phi_k, \quad (2)$$

$$L_g \delta g_k^{\text{nl}} = -(\delta \vec{u}_E \cdot \nabla \delta g), \quad (3)$$

with $L_g = \partial_t + v_\parallel \partial_\parallel + \vec{v}_d \cdot \nabla$ and standard notations. In the linear limit, Eq. (1) can be formally written as $(eN_{e0}/T_e) L_k \Phi = 0$, with L_k the linear eigenmode operator. Specifically, we note that $L_0 \Phi(z_0) = L_1 \Phi(z_1) = 0$. Here, we assume that $\Phi(z)$ is the normalized linear eigenmode, i.e., $\int |\Phi|^2 dz = 1$.

Assuming fluid approximation for δg_k^{nl} on the left-hand side of Eq. (3), consistently with the frequency and wavelength ordering assumed above, we have the following Hasegawa–Mima-like equation,

$$\frac{\partial}{\partial t} L_k \delta\phi_k = \alpha_e \frac{c}{2B} \rho_e^2 (\vec{k}'_\perp \times \vec{k}_\perp) \cdot \vec{e}_\parallel (k''_\perp{}^2 - k'_\perp{}^2) \delta\phi_k \delta\phi_{k''},$$

with $\alpha_e \equiv [\delta P_{\perp,ek}/(eN_{0e} \delta\phi_k) - 1]$, i.e., $\alpha_e = \{\tau(1 + \eta_e)/[(3\tau - 1)L_n/R + 1/2] + 1\}$,¹³ and $\vec{k} = \vec{k}' + \vec{k}''$. Here, \vec{k}' and \vec{k}'' should be strictly interpreted as operators, i.e., $i\vec{k}' \delta\phi_{k'} = \vec{\nabla} \delta\phi_{k'}$.

We now proceed with specific calculations. For the low- n l mode, $k = k_{n_l}$, $k'_\perp = (k_{n_0})_\perp$ and $k''_\perp = -(k_{n_1})_\perp$ [complex conjugate of $(k_{n_1})_\perp$], we can ignore variations on the scale of $1/n_l q'$ and concentrate only on the $j=0$ term,

$$\frac{\partial}{\partial t} L_l a_l(t) \Phi_{l0}(r) = i a_0 a_1^* \hat{\alpha}_e \left(\frac{k_{\theta 0}}{\Delta_0} \right) \frac{\partial}{\partial z_0} [\delta k_\perp^2]_0 \Psi_0,$$

where $a_k = eA_k/T_e$, $\hat{\alpha}_e = \alpha_e |\Omega_e| \rho_e^4$, $\Psi_0 = \sum_j |\Phi_{0j}|^2$, $\Phi_{0j} = \Phi(z_0 - j)$, and

$$\begin{aligned}
[\delta k_{\perp}^2]_0 \Psi_0 &= \frac{2n_l}{n_0} k_{\theta 0}^2 (1 + \hat{s}^2/W_0^2) \Psi_0 \\
&\equiv \frac{2n_l}{n_0} k_{\theta 0}^2 \Psi_0 + q_s'^2 \sum_j n_1^2 \Phi_{0j} \frac{\partial^2}{\partial z_0^2} \Phi_{0j}^* \\
&\quad - n_0^2 \Phi_{0j}^* \frac{\partial^2}{\partial z_0^2} \Phi_{0j},
\end{aligned}$$

where we have considered $k_{\theta 1} \approx k_{\theta 0}$ and $k_{\theta l} \equiv k_{\theta 0} - k_{\theta 1} = k_{\theta 0}(n_l/n_0)$. Furthermore, $\hat{s} = r_s q_s' / q_s$, and $W_0 \sim O(1)$ denotes the typical width of $\Phi(z_0)$. Strictly speaking, $1/W_0$ must be considered as an operator, as it is implicitly assumed without loss of generality in its definition above. Noting $L_l \approx \tau$, and defining $\Phi_{l0}(r) = i(\partial/\partial z_0)(1 + \hat{s}^2/W_0^2)\Psi_0$, we have,

$$\frac{\partial a_l(t)}{\partial t} = \frac{\hat{\alpha}_e}{\tau} \frac{2n_l}{n_0} \frac{k_{\theta 0}^3}{\Delta_0} a_0 a_1^*. \quad (4)$$

The feedback equation for the pump mode $\delta\phi_0$, using $k = k_{n_0}$, $k' = k_{n_1}$, and $k'' = k_{n_l}$, is given by

$$\frac{\partial}{\partial t} L_0 a_0(t) \Phi(z_0) = \hat{\alpha}_e a_1 a_l \frac{k_{\theta 1}}{\Delta_1} [k_{\perp 1}^2] \Phi(z_0) \frac{\partial^2}{\partial z_0^2} \left(1 + \frac{\hat{s}^2}{W_0^2}\right) \Psi_0,$$

with $[k_{\perp 1}^2] f(z_0) g(z_0) \equiv -k_{\theta 1}^2 [g(1 - \hat{s}^2 \partial^2/\partial z_0^2) f + \hat{s}^2 f \partial^2 g/\partial z_0^2]$. Projecting with $\Phi^*(z_0)$, we obtain,

$$(\partial_t - \gamma_0) a_0(t) = -(\hat{\alpha}_e/\tau) a_1 a_l (k_{\theta 1}/\Delta_1) (k_{\perp 1}^2/W_l^2), \quad (5)$$

where γ_0 is the linear growth/damping rate, and

$$(k_{\perp 1}^2/W_l^2) \equiv - \int dz_0 \Phi^* [k_{\perp 1}^2] \Phi \frac{\partial^2}{\partial z_0^2} \left(1 + \frac{\hat{s}^2}{W_0^2}\right) \Psi_0.$$

Thus, W_l corresponds to the typical radial scale of Φ_{l0} or $\delta\phi_l$, and $\omega_0 \partial D_0/\partial \omega_0 \approx \tau$ is noted with D_0 being the Hermitian part of the linear ETG dielectric constant. Following the same procedure, we can readily derive the following evolution equation of another pump mode $a_1(t)$:

$$(\partial_t - \gamma_1) a_1(t) = (\hat{\alpha}_e/\tau) a_0 a_l^* (k_{\theta 0}/\Delta_0) (k_{\perp 0}^2/W_l^2). \quad (6)$$

With evolution equations for a_l , a_0 , a_1 derived, we can readily extend the results to the case of multi- n pump modes interacting with a single n_l quasimode. In this case each n mode will interact with the $n+n_l$ mode, as well as with the $n-n_l$ mode. The a_l mode, meanwhile, will interact with all the n and $n-n_l$ pairs. Noting that $n \gg n_l$, we can take the continuum limit and obtain the final set of spectral-cascading equations for the wave energy density $I_n = |a_n|^2/2$,

$$\left(\frac{\partial}{\partial t} - 2\gamma_n\right) I_n + v_n \frac{\partial}{\partial n} I_n = 0, \quad (7)$$

where $v_n(t) = -(2\hat{\alpha}_e/\tau) \hat{s} k_{\theta n}^2 (k_{\perp n}^2/W_l^2) n_l |a_l(t)|$, and

$$\left(\frac{\partial}{\partial t} + \gamma_l\right) |a_l(t)| = 4(\hat{\alpha}_e/\tau) q_s' \int k_{\theta n}^3 I_n dn. \quad (8)$$

In Eq. (8), we have introduced γ_l as the damping rate of the forced n_l mode via $k_{\parallel} v_{\parallel}$ Landau damping.

Equation (7) indicates cascades toward lower n modes if $v_n < 0$. Meanwhile, $\text{sgn}(v_n) = -\text{sgn}(k_{\perp n}^2)$, and, approximately, $k_{\perp n}^2 \approx k_{\theta n}^2 [\hat{s}^2/W_l^2 - (1 + \hat{s}^2/W_n^2)]$. Here, we recall that W_l and

W_n are, respectively, the radial scales of Φ_{l0} and Φ_n . Noting, typically $W_n \leq 1$, and $\hat{s} \sim 1$, we have $\Phi_{l0}(r) \sim |\Phi_n(z)|^2$, and hence, $W_l \sim W_n/2$ and $k_{\perp n}^2 > 0$, i.e., $v_n < 0$. So wave energy cascades from high to lower n values. We emphasize that the low- n forced oscillation having rapid radial variation is crucial in terms of, not only determining the direction of the energy cascade, but also the cascading rate, i.e., $|v_n| \sim W_l^{-4}$. Such rapid radial oscillations are, of course, due to the fact that the spontaneously excited pump ETG modes are composed of radially localized poloidal harmonics with nearly flat envelope, i.e., the ballooning-mode structure unique to the toroidal geometry. It is also worthwhile noticing that, in the present analysis leading to Eq. (7), the low- n mode have the role of *mediators* in the spectral cascading: they are unimportant in terms of amplitudes but crucial in the sense they make *nonlocal* transfers of energy possible in wave vector space. The resulting downshifted nonlinear (with respect to the linear) spectrum, see Fig. 1, is characterized by radially elongated-streamer-like structures. Thus these structures can be considered as nonlinear streamers. However, we emphasize that their characteristic radial extension is due to linear toroidal mode couplings, as in the linear phase, since nonlinear distortions to toroidal equilibrium variations is small, as discussed below. Further proof of this are the weak effects of nonlinear dynamics on the streamers envelope structure.

Another important issue to be discussed is the nonlinear generation of $(n, m) = (0, 1)$ low frequency fluctuations by beatings of neighboring poloidal harmonics of the same n . It can be shown that these $(0, 1)$ low frequency quasimodes alter the ETG potential well structure parallel to magnetic field lines and, thus, their parallel mode structure and growth/damping rate. At saturation, the amplitude of $(0, 1)$ low frequency fluctuations is still small compared with toroidal equilibrium variations in the poloidal plane. For this reason, the effect of $(0, 1)$ low frequency modes is marginal on ETG streamers envelope structures. Detailed analysis of these issues will be presented in a future publication.

V. DISCUSSION AND CONCLUSION

Key findings from global gyrokinetic particle simulations are that ETG instability saturates via nonlinear toroidal couplings and that radially extended streamers do not drive a large electron thermal transport expected from mixing length estimates. The nonlinear gyrokinetic theory confirms qualitatively key simulation results, among others, that the ETG spectral energy cascades to lower toroidal mode numbers. Our studies focus on toroidal ETG turbulence with a strong positive magnetic shear $\hat{s} \sim 1$, of which flux-tube simulations predict large electron transport. The mechanism of instability saturation and electron transport could be very different in the weak shear region with $\hat{s} \sim 0$, where the dominant instability is a slab ETG.³⁹

The crucial role of low- n quasimodes as mediators in nonlinear toroidal couplings is a possible explanation of the difference between flux-tube and global simulations. In fact, the quasimode has an optimal mode number $\sim n_0^{1/2}$, where $n_0 \sim 1000$, and a parallel wave vector $\sim 1/qR_0 n_0^{1/2}$ (Sec. IV). Thus, ETG simulations require¹⁶ that radial box size scales

as $\sim \rho_e n_0^{1/2}$ and parallel box size scales as $\sim q R_0 n_0^{1/2}$, i.e., order of magnitude larger than current flux-tube ETG simulations.¹⁵ If quasimode dynamics is suppressed, then only parallel mode structure modification via the (0, 1) mode and zonal flow dynamics can set the (much higher) saturation level of the ETG turbulence. Finally, since all unstable eigenmodes participate in nonlinear toroidal couplings, using a small number of toroidal eigenmodes may not accurately predict the saturation amplitude.

We note that there are accumulating evidences from first-principles turbulence simulations that contradict the heuristic mixing length rule, which underlies most existing transport models. We have reported earlier²¹ a gradual transition from Bohm to gyro-Bohm scaling for the ion transport driven by the ITG turbulence although the eddies are isotropic. In this paper, we further demonstrate that the scaling of electron transport driven by the ETG turbulence is gyro-Bohm even though the size of streamers scales with the device size. The key to reconciling these obvious contradictions is that transport is diffusive and driven by the local fluctuation intensity, rather than the eddy size. The deviation of ITG transport from the gyro-Bohm scaling is due to the fact that the fluctuation intensity is driven by nonlocal effects, i.e., the turbulence spreading.^{21,40,41} Meanwhile, the ETG fluctuation intensity is determined by the nonlinear toroidal coupling, which does not depend on the streamer (or system) size. The effects of turbulence spreading is negligible in ETG since the fluctuation intensity is independent of the device size.

In conclusion, global gyrokinetic particle simulation and nonlinear gyrokinetic theory find that ETG instability saturates via nonlinear toroidal couplings, which transfer energy successively from unstable modes to damped modes preferably with lower toroidal mode numbers. The electrostatic ETG turbulence is dominated by nonlinearly generated radial streamers with an eddy turnover time much longer than the linear growth time. The streamer length scales with the device size and is longer than the distance between mode rational surfaces and electron radial excursions. Both fluctuation intensity and transport level at saturation are independent of the streamer size. The nonlinear toroidal couplings represent a new paradigm for regulating turbulence via the toroidal spectral cascade.

ACKNOWLEDGMENTS

Z.L. acknowledges useful discussions with T. S. Hahm, P. H. Diamond, W. W. Lee, and W. M. Tang. This work was supported by U.S. Department of Energy Cooperative Agree-

ment No. DE-FC02-04ER54796, DOE Contract No. DE-FG03-94ER54271 and 54736, and by the DOE SciDAC GPS Center. Simulations were performed using the IBM SP computer at NERSC.

- ¹W. M. Tang, Nucl. Fusion **18**, 1089 (1978).
- ²F. Ryter *et al.*, Nucl. Fusion **43**, 1396 (2003).
- ³A. Manini *et al.*, Plasma Phys. Controlled Fusion **46**, 1723 (2004).
- ⁴A. Bottino, Ph.D. thesis, EPFL, Lausanne, Switzerland, 2004.
- ⁵G. T. Hoang *et al.*, Phys. Rev. Lett. **87**, 125001 (2001).
- ⁶W. Horton *et al.*, Phys. Plasmas **11**, 2600 (2004).
- ⁷K. L. Wong *et al.*, Phys. Lett. A **276**, 281 (2000).
- ⁸A. B. Rechester and M. N. Rosenbluth, Phys. Rev. Lett. **40**, 38 (1978); J. D. Callen, *ibid.* **94**, 055002 (2005).
- ⁹W. Horton *et al.*, Phys. Fluids **31**, 2971 (1988).
- ¹⁰B. B. Kadomtsev, *Plasma Turbulence* (Academic, London, 1965).
- ¹¹Z. Lin *et al.*, Science **281**, 1835 (1998).
- ¹²P. H. Diamond *et al.*, Proceedings of the 17th International Conference on Controlled Fusion and Plasma Physics, Yokohama, Japan, 1998.
- ¹³Liu Chen *et al.*, Phys. Plasmas **7**, 3129 (2000).
- ¹⁴A. Hasegawa and K. Mima, Phys. Rev. Lett. **39**, 205 (1977).
- ¹⁵F. Jenko *et al.*, Phys. Plasmas **7**, 1904 (2000); W. Dorland *et al.*, Phys. Rev. Lett. **85**, 5579 (2000).
- ¹⁶M. A. Beer *et al.*, Phys. Plasmas **2**, 2687 (1995).
- ¹⁷B. Labit and M. Ottaviani, Phys. Plasmas **10**, 126 (2003).
- ¹⁸J. Li and Y. Kishimoto, Phys. Plasmas **11**, 1493 (2004).
- ¹⁹S. C. Cowley *et al.*, Phys. Fluids B **3**, 2767 (1991).
- ²⁰H. Bigrari *et al.*, Phys. Fluids B **2**, 1 (1990).
- ²¹Z. Lin *et al.*, Phys. Rev. Lett. **88**, 195004 (2002); Phys. Plasmas **11**, 1099 (2004).
- ²²R. B. White (private communication).
- ²³W. W. Lee, Phys. Fluids **26**, 556 (1983); J. Comput. Phys. **72**, 243 (1987).
- ²⁴N. Metropolis *et al.*, J. Chem. Phys. **21**, 1087 (1953).
- ²⁵Z. Lin *et al.*, Phys. Rev. Lett. **83**, 3645 (1999); Phys. Plasmas **7**, 1857 (2000).
- ²⁶S. E. Parker *et al.*, Phys. Rev. Lett. **71**, 2042 (1993).
- ²⁷W. W. Lee and R. A. Santoro, Phys. Plasmas **4**, 169 (1997).
- ²⁸S. E. Parker *et al.*, Phys. Plasmas **11**, 2594 (2004).
- ²⁹A. M. Dimits, Ph.D. thesis, Princeton University, 1988.
- ³⁰L. Villard *et al.*, Nucl. Fusion **44**, 172 (2004).
- ³¹C. Holland and P. H. Diamond, Phys. Plasmas **11**, 1043 (2004).
- ³²R. D. Sydora *et al.*, Plasma Phys. Controlled Fusion **38**, A281 (1996).
- ³³W. M. Tang and G. Rewoldt, Phys. Fluids B **5**, 2451 (1993).
- ³⁴F. Romanelli and F. Zonca, Phys. Fluids B **5**, 4081 (1993).
- ³⁵R. Z. Sagdeev and A. A. Galeev, *Nonlinear Plasma Theory* (Benjamin, New York, 1969); P. L. Similon and P. H. Diamond, Phys. Fluids **27**, 916 (1984); T. S. Hahm and W. M. Tang, Phys. Fluids B **3**, 989 (1991).
- ³⁶J. W. Connor *et al.*, Proc. R. Soc. London **365**, 1 (1979); Y. C. Lee and J. W. Van Dam, Finite Beta Theory Workshop, Varenna, (1979); A. H. Glasser, *ibid.* (1979).
- ³⁷F. L. Hinton and M. N. Rosenbluth, Plasma Phys. Controlled Fusion **41**, A653 (1999).
- ³⁸E. A. Frieman and L. Chen, Phys. Fluids **25**, 502 (1982).
- ³⁹Y. Idomura and M. Wakatani, Phys. Plasmas **7**, 3551 (2000).
- ⁴⁰T. S. Hahm *et al.*, Plasma Phys. Controlled Fusion **46**, A323 (2004); O. Gurcan *et al.*, Phys. Plasmas **12**, 032303 (2005).
- ⁴¹L. Chen *et al.*, Phys. Rev. Lett. **92**, 075004 (2004); F. Zonca *et al.*, Phys. Plasmas **11**, 2488 (2004); R. B. White *et al.*, *ibid.* **12**, 057304 (2005).